Wlodek, M., Kolasińska-Sojka, M., Szuwarzyński, M., Kereïche, S., Kováčik, L., Zhou, L., Islas Flores, L. E., Warszyński, P., & Briscoe, W. H. (2018). Supported lipid bilayers with encapsulated quantum dots (QDs) via liposome fusion: Effect of QD size on bilayer formation and structure. *Nanoscale*, *10*(37), 17965-17974. https://doi.org/10.1039/C8NR05877F

Nanoscale

Accepted Manuscript

This article can be cited before page numbers have been issued, to do this please use: M. Wlodek, M. Kolasiska-Sojka, M. Szuwarzyski, S. Kereïche, L. Kováik, L. Zhou, L. Islas, P. Warszyski and W. H. Briscoe, *Nanoscale*, 2018, DOI: 10.1039/C8NR05877F.

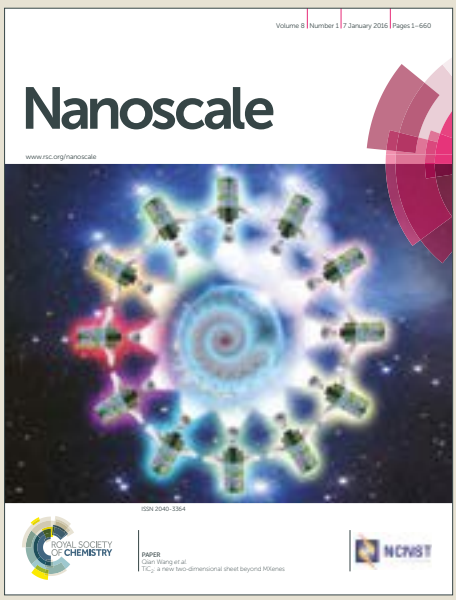

ROYAL SOCIETY OF CHEMISTRY

rsc.li/nanoscale

View Article Online
DOI: 10.1039/C8NR05877F

Nanoscale

ARTICLE

Supported lipid bilayers with encapsulated quantum dots (QDs) *via* liposome fusion: Effect of QD size on bilayer formation and structure

Received 00th January 20xx,
Accepted 00th January 20xx

DOI: 10.1039/x0xx00000x

www.rsc.org/

Magdalena Wlodek,*[a] Marta Kolasinska-Sojka,*[a] Michal Szuwarzynski, [b] Sami Kereïche, [c] Lubomir Kovacik, [d] Liangzhi Zhou, [e] Luisa Islas, [e] Piotr Warszynski [a] and Wuge H. Briscoe*[e]

Understanding interactions between functional nanoparticles and lipid bilayers is important to many emerging biomedical and bioanalytical applications. In this paper, we report incorporation of hydrophobic cadmium sulphide quantum dots (CdS QDs) into mixed 1-palmitoyl-2-oleoyl-sn-glycero-3-phosphocholine (POPC) / 1-palmitoyl-2-oleoyl-sn-glycero-3-phosphoethanolamine (POPE) liposomes, and into their supported bilayers (SLBs). The QDs were found embedded in the hydrophobic regions of the liposomes and the supported bilayers, which retained the QD fluorescent properties. In particular, we studied the effect of the QD size (2.7–5.4 nm in diameter) on the formation kinetics and structure of the supported POPC/POPE bilayers, monitored *in situ* using quartz crystal microbalance with dissipation monitoring (QCM-D), as the liposomes ruptured onto the substrate. The morphology of the obtained QD-lipid hybrid bilayers was studied using atomic force microscopy (AFM), and their structure by synchrotron X-ray reflectivity (XRR). It was shown that the incorporation of hydrophobic QDs promoted bilayer formation on the PEI cushion, evident from the rupture and fusion of the QD-endowed liposomes at a lower surface coverage compared to the liposomes without QDs. Furthermore, the degree of disruption in the supported bilayer structure caused by the QDs was found to be correlated with the QD size. Our results provide mechanistic insights into the kinetics of the rupturing and formation process of QD-endowed supported lipid bilayers *via* liposome fusion on polymer cushions.

Introduction

The development of nanoparticles (NPs) as a delivery vector for therapeutic agents has introduced new opportunities for medical treatment[1] and bio-sensing.[2,3] For example, hydrophobic NPs (superparamagnetic iron oxide nanoparticles SPIONs) have been employed in nanostructured assemblies for therapeutic controlled delivery systems.[4] Quantum dots (QDs) are among the most promising NPs due to their unique photophysical properties, including a high fluorescence quantum yield; long fluorescence lifetime; strong and size-dependent tunable photoluminescence; and a broad absorption and narrow emission spectra.[5–7] QDs have been designed for targeted drug delivery (principally anticancer drugs) [8,9], and for cell imaging (especially for labeling cells and vesicle membranes).[10,11] However, most highly luminescent QDs can only be dispersed in non-polar solvents,[12] and their hydrophobicity introduces serious limitations for their biomedical and clinical applications. Their toxicity is also a concern; for instance, cadmium containing QDs are cytotoxic[13] not only due to the release of Cd^{2+} ions, but also due to the intracellular distribution of the QDs and associated nanoscale effects.[14]

To overcome these limitations, surface modification is often necessary for QDs to be dispersed in aqueous solutions and achieve biocompatibility.[15] One of the most promising pathways to achieve this is to encapsulate the QDs into liposomes.[16,17] However, the insertion of the hydrophobic NPs into the nonpolar interior of the lipid bilayer is limited by the thickness of the lipid membrane, and only QDs smaller than 5 nm could be readily embedded in the hydrophobic part of the bilayer.[18,19] In the case of hydrophobic QDs larger than ~6 nm, phospholipid micelle formation was observed, where the QDs were embedded in the hydrophobic micelle interior.[19,20]

A number of QDs such as CdSe,[21] CdSe/ZnS,[22,23] CdSe/CdZnS,[16] CdTe,[17,24] and carbon[25] have been embedded into the hydrophobic tail region of liposomes without

[a] Jerzy Haber Institute of Catalysis and Surface Chemistry, Polish Academy of Sciences, Niezapominajek 8 PL-30239 Krakow, Poland.
[b] AGH University of Science and Technology, Academic Centre for Materials and Nanotechnology, al. A. Mickiewicza 30, PL-30059 Krakow, Poland.
[c] Institute of Biology and Medical Genetics, First Faculty of Medicine, Charles University, Albertov 4, 128 01Prague 2, Czech Republic.
[d] Center for Cellular Imaging and NanoAnalytics (C-CINA), Biozentrum, University of Basel, Mattenstrasse 26, CH-4058 Basel, Switzerland.
[e] School of Chemistry, University of Bristol, Cantock's Close, Bristol BS8 1TS, United Kingdom.
* E-mail: ncwlodek@cyf-kr.edu.pl (MW); nckolasi@cyf-kr.edu.pl (MKS); wuge.briscoe@bristol.ac.uk (WHB)
Electronic Supplementary Information (ESI) available: [details of any supplementary information available should be included here]. See DOI: 10.1039/x0xx00000x

View Article Online
DOI: 10.1039/C8NR05877F

significantly compromising the liposome structure. Nonspecific QD adsorption to pre-formed supported lipid bilayers (SLBs)[26] and polyelectrolyte multilayers (PEMs)[27] has also been previously studied. However, the formation and structure of QD-embedded SLBs *via* the fusion of QD-endowed liposomes has not been reported, which is the focus of the current study. SLB-QDs hybrids represent a promising platform in biotechnology, for instance for novel devices with features of flexible structures such as single-electron transistors, plasmonic devices and biotransistors.[28,29] Moreover, SLB-QDs are also relevant to tracking of the vesicle fusion on surfaces *via* fluorescence visualization of the QDs in the resulting bilayer patches.[30] Such studies are also relevant to understanding the interactions between functional NPs and model cell membranes, which is crucial to the design and use of nanomaterials in many biomedical applications where nanotoxicity should be minimized.[31] Key mechanisms of the interactions between NPs and cell membranes may be revealed using cell membrane models such as lipid vesicles or planar lipid structures (SLBs and Langmuir monolayer) and more recently developed computational models. Thus, biomimetic membrane models are interesting candidates for studying and understanding the NP interaction with cell membranes, which plays a central role in NP in vivo activity.[32,33] Theoretical and computer simulation studies have examined NP attachment or adsorption to SLBs. These studies have shown that NPs could induce disruptions and pore formation of the lipid bilayers depending on their size and surface chemistry,[34,35] causing nanoscale hole formations and membrane thinning.[36,37] Experimentally, it has been observed that embedded NPs could either improve or disrupt bilayer ordering, and also change membrane phase behaviour. Bothun *et al*.[38] demonstrated that the incorporation of hydrophobic NPs into a liposomal membrane decreased its melting temperature at high lipid to NP ratios due to an increase in the bilayer fluidity of the gel phase caused by a reduction in lipid ordering. Park *et al.*[39,40] using fluorescence anisotropy, found that hydrophobic silver and gold NPs increased the DPPC membrane fluidity and decreased its phase transition temperature. High pressure small angle X-ray scattering (HP-SAXS) experiments showed that 10 nm hydrophobic SiO_2 NPs promoted lamellar to inverted hexagonal transitions in phospholipid dioleoyl phosphatidylethanolamine (DOPE) mesophases,[41] whilst 10 nm hydrophilic SiO_2 NPs stabilized monoolein (MO) mesophase curvature at low NP concentrations, but disrupted mesophase order at high NP concentrations.[42] However, our knowledge remains limited regarding the influence of hydrophobic nanoparticles on the formation of SLBs *via* liposome (or vesicle) fusion. In particular, it is not well understood how the presence of NPs might influence the reorganization and evolution of the structure and morphology of SLBs.

Here, we have studied the impact of hydrophobic NPs on the formation and structure of mixed 1-palmitoyl-2-oleoyl-sn-glycero-3-phosphocholine (POPC) / 1-palmitoyl-2-oleoyl-sn-glycero-3-phosphoethanolamine (POPE) lipid bilayers, formed by liposome fusion atop a positively charged polyethyleneimine (PEI) monolayer. POPC and POPE are common lipids found in bacterial and eukaryote membranes,[43] and their mixed bilayers have been widely studied as model membranes. Moreover, hydrogen bonding formation among PE lipids and between the PE headgroup and the solid support could promote vesicle fusion and SLB formation.[44,45] The PEI film has been previously shown[46–50] as an effective anchor for subsequent adsorption of nanoobjects such as polyelectrolytes, nanoparticles, or liposomes. In our study, the PEI monolayer preparation used the same procedure as that in these studies, and the detailed characterization of such PEI monolayers has also been reported by Adamczyk *et al.*.[51] The control surface topography AFM image and XRR curve for the PEI on silica are shown in Figure S5 and S6, respectively in the SI section. Hydrophobic cadmium sulphide (CdS) QDs of size 2.7, 3.8, 4.9 and 5.4 nm were used in this study, and their incorporation into the lipid bilayer during liposome preparation was confirmed by cryo-TEM imaging. Fluorimetric emission spectra further confirmed the QD presence in the POPC/POPE liposomes and in the SLBs formed by liposome fusion on the PEI monolayer. The kinetics of liposome deposition on the PEI film and subsequent SLB formation were monitored by quartz crystal microbalance (QCM-D). Furthermore, the influence of embedded QDs on the SLB structure and topography was studied using synchrotron X-ray reflectivity (XRR) and atomic force microscopy (AFM), respectively. Our results demonstrate that all hydrophobic CdS QDs with a size of 2.7–5.4 nm could be successfully incorporated in the POPC/POPE liposomes and SLBs to improve their compatibility with aqueous environments, which is a key requirement for the application of such QD-lipid hybrids as functional nanomaterials. This shows that the fusion *via* QD-endowed liposomes is a viable route to form fluorescent QD-embedded SLBs. Our findings on the effect of the QD size (as model NPs) on the lipid bilayer structure are also relevant to the fundamental understanding of interactions between NPs and lipid membranes.

Materials and Methods

Materials and sample preparation

Branched poly(ethyleneimine) (PEI, M_w 750 kDa) was obtained from Sigma-Aldrich (Germany). POPC and POPE were purchased from Avanti Polar Lipids. CdS QDs stabilized with oleic acid and of diameter 2.7, 3.8, 4.9, and 5.4 nm were purchased from Aldrich, and were received as suspensions at 5 mg mL^{-1} in toluene.

NaCl (99.5%) used for preparing PEI solutions was obtained from Fluka. H_2SO_4 (96%) and H_2O_2 (32%) used for the cleaning procedure of the silicon/quartz crystals were purchased from Aldrich. Phosphate buffer (PBS) was made from NaCl, Na_2HPO_4, and NaH_2PO_4, with the pH adjusted to 9.5 by the addition of NaOH. Ultrapure, Millipore water with resistivity > 18 MΩ cm was used for all solution preparation. Silicon wafers (On semiconductor, Czech Republic), freshly cleaved natural ruby mica (from Dean Transted, England), and standard

View Article Online
DOI: 10.1039/C8NR05877F

gold/quartz sensors QSX 301 (Q-Sense, Sweden) were pre-coated with PEI by dipping them into the polymer solutions (0.5 mg mL^{-1}) for 15 min, then rinsed in water (3 times) and used as supports for the QD-vesicles deposition. Gold/quartz crystals and Si wafers were cleaned before use with piranha solution, which is a mixture of equivalent volumes of concentrated sulfuric acid and hydrogen peroxide. *(Caution! This solution is a very strong oxidizing agent and should be handled carefully).* Substrates were dipped into piranha solution for 30 min and then carefully rinsed with Milli-Q water, followed by 30 min dipping into hot (ca. 70°C) Milli-Q water.

Preparation of liposomes with quantum dots: *Liposomes with QDs* were prepared using a thin film hydration method. Typically, 150 µL of a CdS QD (of a designated size) suspension in toluene (5 mg mL^{-1}) was mixed with 5 mg of POPC and 5 mg of POPE phospholipids in 850 µL of chloroform. Assuming the QD density of 4.82 g cm^{-3}, this corresponds to a QD-lipid number ratio of v = 1.9×10^{-3} (for 2.7 nm QDs), 6.6×10^{-4} (3.8 nm), 3.1×10^{-4} (4.9 nm), 2.3×10^{-4} (5.4 nm) or a volume ratio of ϕ = 1.4×10^{-2}. We used this optimized lipid-QD ratio with a number of considerations. First, it is comparable to the upper range of those investigated in a number of previous studies, where the strongest effects on NP-membrane interactions number ratios have been observed.[41,42] Secondly, this QD concentration was optimized to give the highest fluorescence intensity. For higher QD concentrations, it became more difficult for extruding liposomes through polycarbonate membranes and QD residues were also observed on the extrusion membranes. For lower QD concentrations, the measured fluorescence intensity was weaker. This yielded a lipid:QD mixed solution with a QD concentration of 0.75 mg mL^{-1}. Then, the solvent was evaporated under vacuum overnight. The dried film was hydrated in 2 mL phosphate buffer of ionic strength 0.2 M and pH = 9.5. The obtained multilamellar vesicles (MLV) were further ultrasonicated with a sonicator bath for 20 min at room temperature. The resulting suspension was extruded 15 times through a polycarbonate membrane with nominally 200 nm pores, and then a further 15 times *via* a membrane with 100 nm pores using a mini-extruder (Avanti Polar Lipids). The obtained suspension of *small unilamellar vesicles with QDs* (SUV-QDs) was then diluted to the final lipid concentration of 0.4 mg mL^{-1}. Dynamic light scattering (DLS) measurements gave the average diameter d_L for the liposomes to be ~90.2±6.0 nm, and for the SUV-QDs ~110±10 nm for all four QD sizes. The zeta potential for all the liposomes (with and without QDs) was −19.0±1.1 mV. The DLS results are presented in SI section SI.2.

Experimental techniques

Transmission Cryo-Electron Microscopy (Cryo-TEM)

Cryo-TEM measurements were carried out on a Tecnai G2 Sphera 20 electron microscope (FEI Company, Hillsboro, OR, USA) equipped with a LaB6 gun and Gatan 626 cryo-specimen holder (Gatan, Pleasanton, CA, USA). The sample preparation and imaging details are given in the Supporting Information (SI) section SI.1. All cryo-TEM pictures were carefully inspected for possible artifacts such as radiation damage and ice crystals, and high-quality images were CTF-corrected and band-pass filtered to suppress ice thickness variations and noise below 1 nm detail size.

Fluorescence emission spectra

The fluorescence emission spectra of the CdS QDs in toluene or within POPC/POPE liposomes and SLBs were acquired with a spectrofluorimeter (FluoroLog-3, Horiba, Jobin Yvon) equipped with a xenon lamp as light source. All the samples were excited using 300 nm wavelength light illumination. Quartz cuvettes with a 1 cm path length were used, and excitation and emission slit widths were 3 and 4.5 nm respectively, depending on the sample fluorescence. In the case of the SLBs with QDs, the measurements were performed with an excitation and emission slit width of 5 nm. The films were formed on mica sheets and measured in a dedicated solid-sample holder designed for thin films.

Quartz Crystal Microbalance

The deposition of POPC/POPE liposomes with and without different sizes of QDs on the PEI monolayer was studied *in situ* using the QCM-D (QSense AB Gothenburg, Sweden, present name: Biolin Scientific) at 25°C. The crystals modified with a PEI monolayer were mounted in the flow chamber of the instrument. After resonance frequency calibration, the chamber was filled with the phosphate buffer to obtain a baseline. Then, the liposome dispersion was introduced, and the adsorption kinetics were monitored *in situ*. After obtaining a constant value of resonance frequency, the chamber was rinsed with PBS buffer. The Voigt viscoelastic model, implemented in QTools 3 software, Q-Sense AB, Gothenburg,[52] was used to interpret the experimental data. The deviation in the results from 4 repeated measurements for each liposome samples was within 10%.

Atomic Force Microscopy

AFM images of SLBs with QDs of different sizes on the PEI monolayer were obtained with a Dimension Icon atomic force microscope (Bruker, Santa Barbara, CA) working in the fluid in the Peak Force Tapping™ (PFT) mode. Standard silicon cantilevers for PFT in fluids (Bruker) with a nominal spring constant of 0.7 N m^{-1} and a tip radius <10 nm were used for these measurements. SLBs with QDs were formed by incubating a silicon substrate coated with PEI in the SUV-QD dispersion for 3 h. The substrate was then rinsed with PBS buffer, and the AFM imaging was performed immediately afterwards in PBS.

Synchrotron X-ray reflectometry (XRR) measurements

Grazing incidence X-reflectivity measurements were performed at beamline BM28-XMas at the European Synchrotron Radiation Facility (ESRF), Grenoble, France using an X-ray beam with an energy of 14 keV and a corresponding wavelength λ = 0.886 Å. The measurements were carried out within a sealed cell which allowed temperature control and *in*

View Article Online
DOI: 10.1039/C8NR05877F

situ solution exchange.[53–56] The SLBs were formed by incubating PEI-coated silicon/silica substrates in SUV-QDs dispersion for 3 h and then rinsing with PBS. XRR data was plotted as the reflectivity, R, against momentum transfer vector along the perpendicular direction of the sample surface, $Q = 4\pi/\lambda\, sin(2\theta_i/2)$ where θ_i is the angle of incidence. The measured reflectivity curves were analyzed by applying a standard fitting program Motofit[57] in IGOR Pro (WaveMetrics, Portland, USA). The obtained reflectivity curves were optimised by the least χ^2 method using the Abeles formulation that provides that same results as the Parrat algorithm as implemented in Motofit, in which the SLB with QDs on PEI coated silica were treated as slabs of different scattering densities (SLDs). The fit to experimental data was best described using a six-slab model, consisting of **(1)** the outer headgroup layer exposed to the aqueous environment, **(2)** the outer hydrocarbon chain layer, **(3)** the inner hydrocarbon chain layer, **(4)** the inner headgroup layer, **(5)** the PEI layer, and **(6)** the silicon oxide layer. The obtained fitting parameters allowed us to compare structural differences of the lipid bilayers as a function of the size of the incorporated QDs.

Results and Discussion

Characterization of QD-liposomes

To verify the QD presence and their location in the liposome lipid bilayer, cryo-TEM imaging was performed. The cryo-TEM image in Figure 1(A) shows that liposomes without QDs had an average size of d_L ~100 nm (compared to DLS d_L ~90.2±6.0 nm) and a well-defined lipid bilayer membrane of 4–5 nm in thickness. To ascertain whether the QDs were located within the bilayer or in the liposome cavity was not trivial. The SUV-QDs (Figure 1(B-E)) appeared spherical with an average size d_L ~110 nm, similar to the DLS d_L value, and their membranes appeared darker compared to the control liposomes in Figure 1(A). Some dark dots were also clearly visible, highlighting the circular contour of the liposome membrane (Figure 1(B-E), e.g. red arrows). This is attributed to the embedded QDs within the POPC/POPE lipid bilayer, since they have a higher electron density than the lipid alkyl chains. The liposome membranes became increasingly "blurrier" with the increasing QD size. While the membrane thickness and image sharpness for the liposomes with 2.7 and 3.8 nm QDs were similar to that of the control, the membranes of liposomes embedded with 4.9 and 5.4 nm QDs appeared fuzzier. This indicates that the QDs located within the liposome lipid bilayer modified the liposome structure, consistent with the observation by Al-Jamal *et al.*[58] of deformations of DOPC liposomes caused by CdSe/Zn QD incorporation at low lipid/QD ratios. Moreover, the membrane appeared darker than the liposome cavity, which confirms that the QDs were embedded within the lipid bilayers instead of the cavity. This is also in agreement with the study by Kethineedi *et al.*[59], who observed darker rims of liposomes than the liposome interior upon incorporation of hydrophobic CdSe/ZnS QDs.

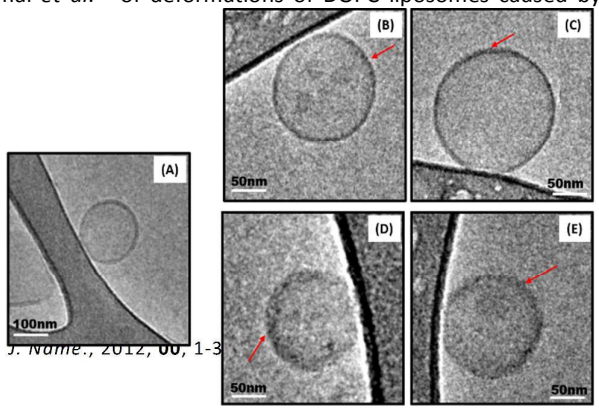

Figure 1. Cryo-TEM images of POPC/POPE liposomes without QDs (A) and with 2.7 nm (B); 3.8 nm (C); 4.9 nm (D); 5.4 nm (E) QDs.

The fluorescence emission spectra were collected to characterize the fluorescent properties of the QD-embedded POPC/POPE liposomes. For reference, fluorescence of the suspensions of all the QDs in toluene was first determined, at a QD concentration of 0.75 mg mL^{-1}, which is the same as that used for the formation of SUV-QDs. The resulting spectra are illustrated in Figure 2(A), showing emission maxima at wavelength λ = 393 nm (for QD diameter d = 2.7 nm), λ = 419 nm (d = 3.8 nm), λ = 449 nm (d = 4.9 nm) and λ = 469 nm (d = 5.4 nm), consistent with the values reported in Ref.[60] The fluorescence emission spectra of the POPC/POPE SUV-QDs in a PBS buffer solution are shown in Figure 2(B).

A comparison between Figure 2(A) and (B) confirms that the QDs of each size were successfully encapsulated in the POPC/POPE SUVs or liposomes, as indicated by the presence of the characteristic QD emission peaks. That is, the SUV-QDs retained the fluorescent properties of the QDs. In the case of the 2.7, 3.8 and 4.9 nm QDs, a gradual increase in the emission spectra at longer wavelengths (λ > 440 nm) was observed,

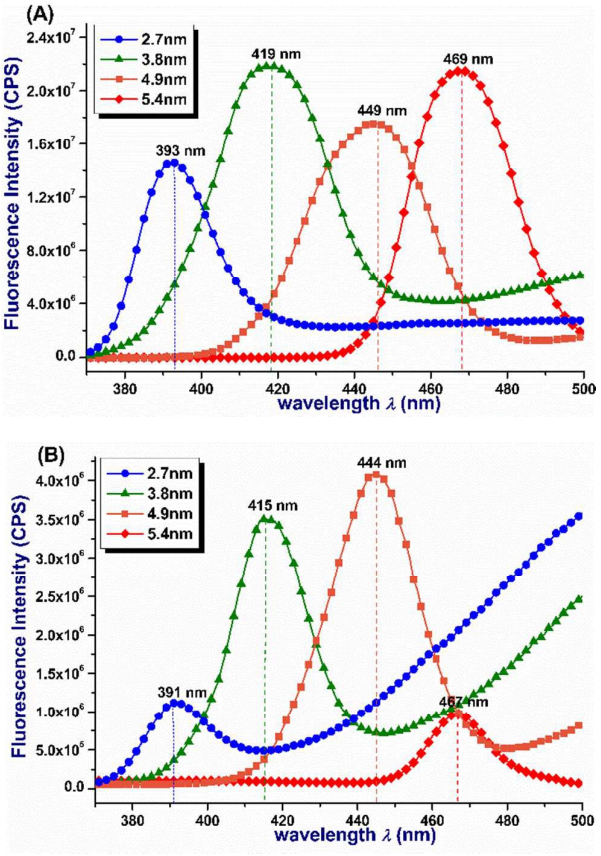

Figure 2. Emission spectra (intensity in counts per second (CPS) vs wavelength λ) of QDs in toluene (A) and POPC/POPE SUV-QDs in aqueous dispersions (B).

View Article Online
DOI: 10.1039/C8NR05877F

which could be attributed to surface defects induced by interactions between the hydrophobic coating on the surface of the QDs and the acyl tails of the POPC/POPE lipids. This is most prominent for smaller QDs because of their larger surface/volume ratio.[61] After the QD incorporation within the liposomes, the fluorescence intensity of the samples was readily detectable but reduced by an order of magnitude compared to the reference in toluene. This could have two causes: some QDs losses during liposome preparation by extrusion, and aggregation of CdS QDs in the lipid bilayer (cf. darkened liposome rims in Figure 1 above) which could lead to QD self-fluorescence quenching.[62] Furthermore, the emission peaks were slightly shifted towards the shorter wavelengths by $\Delta\lambda$ ~2–5 nm relative to the QD spectra in toluene. Such a blue shift has been previously reported for soybean lecithin liposomes with two different sizes of CdSe/ZnS QDs.[63] These changes in the QD optical properties can be attributed to the change in the polarity of the medium to which the QDs were exposed to (i.e. toluene *vs*. the hydrophobic tails of the bilayers), and also to the confinement of the QDs in the bilayer,[63,64] leading to changes in the QD electric surface potential and shifts in the QD energy levels. Furthermore, the concentration of QDs in the liposomes may be estimated by comparing the fluorescence emission peak intensities with those in the reference samples in toluene, assuming no individual hydrophobic QDs were dispersed in the aqueous medium to contribute to the fluorescence emission. For the reference sample in toluene, one can calculate the number of particles per unit volume as $n_{CdS} = c_{CdS}/m_p$, where n_{CdS} is the number of the CdS QD per unit volume in cm^{-3}, c_{CdS} the concentration of particles in the suspension expressed as mass per unit volume in mg mL^{-1}, and m_p is the mass of a single CdS particle in g. The mass of the single CdS particle is given by $m_p = \rho_{QD}V = \rho_{QD}\pi d^3/6$, where $\rho_{QD} = 4.82$ g cm^{-3} is the CdS QD mass density,[65] V the volume of a single CdS particle in cm^3, and d the QD diameter in nm. This gives the mass of the single particle m_p = 4.96×10^{-20} g (for 2.7 nm QDs), 1.38×10^{-19} g (3.8 nm), 2.97×10^{-19} g (4.9 nm), and 3.97×10^{-19} g (5.4 nm), respectively. Using these values and comparing the fluorescence emission intensities from the SUV-QDs (Figure 2(B)) and the reference samples in toluene (Figure 2(A)), we estimated the numbers of the QDs in the liposomes n_{CdS} as listed in **Table 1**. The n_{CdS} in liposomes was lower than that in toluene. It should be noted that some of the QDs embedded in the bilayer might become aggregated and thus experience self-quenching, as discussed above. As such, this number is the *effective* QD number that gave rise to the fluorescence emission detected. The highest *effective loading efficiency* f (the ratio between the effective QD number in the liposomes and that in the reference sample) was observed for QDs with intermediate sizes, i.e. d = 3.8 nm and 4.9 nm, similar to the phospholipid membrane thickness (~4.8 nm). This points to a correlation between the QD-bilayer size compatibility and efficient QD loading in liposomes. However, the mechanism for the non-monotonic dependence of the apparent loading efficiency with respect to the QD size remains unclear. One explanation is the possible NP-size-dependent aggregation of QDs inside the bilayer which could cause different fluorescence quenching. It is also possible that QDs of different sizes could have different retention rates in the extruder membrane during the liposome preparation process. While it has been shown that both the membrane bending modulus as well as the NP size affect the wrapping of hydrophilic NPs and, therefore, their ability to interact with the membrane,[66,67] the insertion of hydrophobic NPs inside the membrane could be favoured if the NPs have a size comparable to or significantly lower than the membrane thickness.

Table 1. Fluorescence intensity (FI), concentration of particles (c_{Cds}), number of particles per unit volume for QDs in reference toluene suspension and in POPC/POPE liposomes (n_{Cds}), and effective loading efficiency (f).

CdS diameter d (nm)	FI (Counts per second, (CPS))		c_{Cds} (mg mL^{-1})		n_{Cds} (cm^{-3})		f (%)
	Reference Sample in Toluene	*SUV-QDs*	*Reference Sample in Toluene*	*SUV-QDs*	*Reference Sample in Toluene*	*SUV-QDs*	
2.7	1.46×10^7	1.12×10^6	0.75	0.06	1.51×10^{16}	1.21×10^{15}	**8.0**
3.8	2.18×10^7	3.50×10^6		0.12	5.42×10^{15}	8.70×10^{14}	**16.0**
4.9	1.76×10^7	4.08×10^6		0.17	2.53×10^{15}	5.72×10^{14}	**22.0**
5.4	2.15×10^7	9.71×10^5		0.03	1.89×10^{15}	8.53×10^{13}	**4.5**

Determination of QDs in the Lipid Bilayers Deposited on PEI Monolayer

The SUV-QDs were deposited on a PEI monolayer, and the influence of the incorporated QDs on the formation of the supported lipid bilayer (SLB) and its structure was examined. The fluorescence emission spectra of POPC/POPE liposomes with QDs of four different sizes adsorbed on the PEI monolayer after 3 h incubation are shown in Figure 3. The spectra show

View Article Online
DOI: 10.1039/C8NR05877F

the characteristic CdS QD emission peaks (cf. Table S2), with the slightly red-shifted ($\Delta\lambda < 1$ nm for the QD-SLBs with 2.7 nm, 4.9 nm and 5.4 nm QDs) peak positions and with similar peak widths compared to those of the SUV-QDs in phosphate buffer (Figure 2(B)), but with reduced fluorescence peak intensities. In the case of the QD-SLBs with 3.8 nm QDs, the emission peak was shifted towards the longer wavelengths by $\Delta\lambda \sim 3$ nm. A "red" shift could be caused by aggregation of water-soluble QDs,[62] or confinement-induced QD aggregation.[61] Our QCM-D and XRR results suggest that the most effective QD embedding within lipid bilayers was observed for 3.8 nm QDs, and the consequent crowding of a larger amount of QDs (as compared to three other QD sizes) could cause more pronounced QD aggregation within the bilayer, resulting in a slightly larger red shift in the emission peak position. However, from fluorimetric experiments we could only ascertain the presence of QDs, and the complementary technique such as the cryo-TEM (cf. Figure 1) could not provide conclusive information on the structure of QDs within the bilayer, which remains to be clarified in future experiments. A gradual increase in the fluorescence intensity towards the longer wavelength was also observed, similar to that observed for the SUV-QDs in Figure 2(B). As the AFM and XRR results below will demonstrate, SLB-QDs had formed after 3 h incubation and the fluorescence spectra here show that they retained the QD fluorescent properties. Thus far, there have been relatively few studies reporting fluorescent SLBs

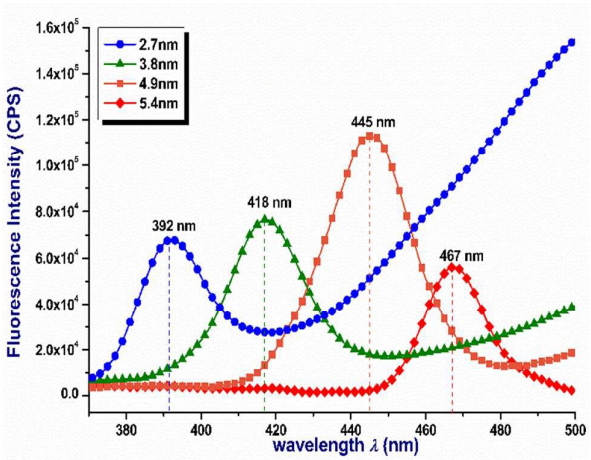

Figure 3. Emission spectra of POPC/POPE SUV-QDs deposited on the PEI monolayer.

formed *via* SUV-QD fusion in the literature.

Effect of QDs on Bilayer Formation and Structure

The interaction between the POPC/POPE SUV-QDs with the positively charged PEI monolayer was studied *in situ* using QCM-D. The quartz crystal resonant frequency shifts Δf as a function of deposition time of the SUV-QDs are shown in Figure 4(A). The frequency decreased initially as a result of liposome adsorption, and then increased towards a plateau value, indicative of liposome rupture and the loss of water from the liposome interior cavity. This shape of Δf vs. time is characteristic of the formation of supported lipid bilayers *via* vesicle fusion.[68–70] Figure 4(B) shows an increase in the corresponding dissipation ΔD as the liposomes adsorbed on the PEI monolayer, and then a decrease in ΔD upon the release of water due to liposome rupture. While the temporal trends in the Δf and ΔD were similar for SUVs with and without QDs, the presence of embedded QDs yielded smaller Δf and ΔD values relative to the liposomes without QDs. This effect was also QD-size dependent, with SUV-QD (2.7 nm) adsorption showing the largest Δf and smallest ΔD values, suggesting a QD-size dependent effect on the SLB formation kinetics and structure. By applying the Voigt viscoelastic model, the final (m_{fin}) and the critical mass (m_Θ) were determined, corresponding to the respective Δf. First, the m_Θ was estimated directly from the depth of the frequency shift minima, Δf_{max}. Next, using the m_Θ value and assuming that the vesicles had an average diameter d_L as measured by DLS and the mass density of water, the number of SUVs (or SUV-QDs) adsorbed per unit area cm^2 was calculated as $n_L = m_\Theta/\rho V$, where the subscript L represents SUVs or SUV-QDs, $V = \pi d_L^3/6$ is the SUV volume, and $\rho = 1$ g mL^{-1} is the mass density of water. Furthermore, the maximum (critical) surface coverage, Θ, could be estimated as $\Theta = n_L \pi d_L^2/4$, and the corresponding area per liposome as $A = 1/n_L$. The obtained results are collected in **Table 2**. A noticeable impact of the embedded QDs on the kinetics of bilayer formation *via* vesicle

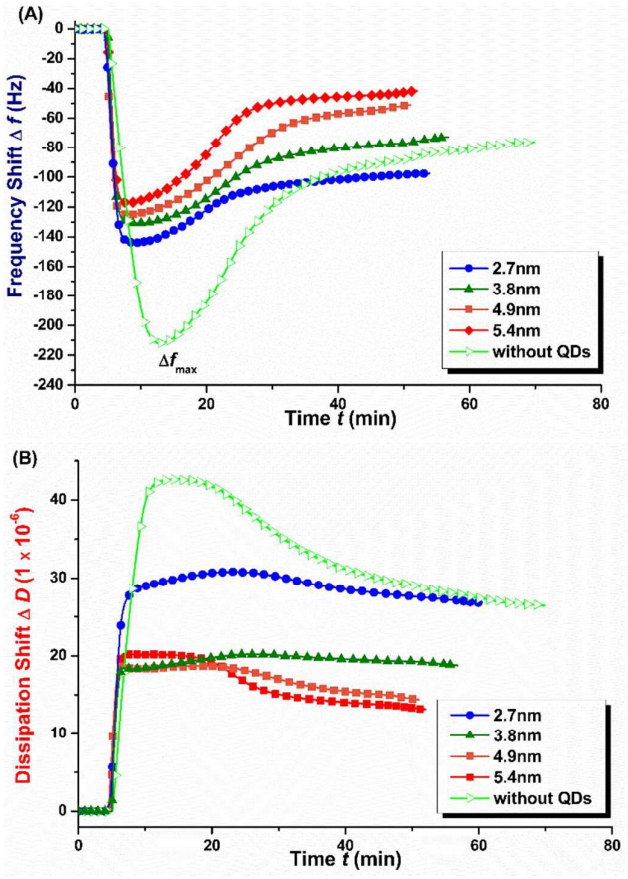

Figure 4. Frequency (A) and dissipation (B) shifts upon the deposition of POPC/POPE liposomes without or with QDs (d = 2.7–5.4 nm) onto PEI monolayer. The fifth overtone is presented.

View Article Online
DOI: 10.1039/C8NR05877F

fusion is evident. The observed Θ values were substantially lower for the SUV-QDs, decreasing with QD diameter *d*. This suggests that the incorporation of the hydrophobic particles had a destabilizing effect on the phospholipid membrane, encouraging vesicle rupture with fusion occurring at a lower surface coverage for SUVs with larger QDs. The projected surface area by a d_L = 110 nm undeformed SUV-QD is A_L ~9.5×10^3 nm^2. The average area *A* occupied by a single SUV-QD ranged from $(15.1–21.6)\times10^3$ nm^2, which is consistent with the picture that the critical liposome coverage was reached below the monolayer coverage for SUV-QD fusion. The results presented in Figure 4 also indicate that the mass of released water was smaller for SUV-QDs as compared with the liposomes without QDs, and the amount of released water increased with the QD size *d* incorporated. There have been a number of studies in the literature investigating the interactions of NPs/QDs with model lipid bilayers such as supported lipid bilayers (SLB) and supported vesicular layers (SVL) using QCM-D.[26,71] However, the effect of embedded hydrophobic NPs/QDs on the formation of supported lipid bilayers *via* vesicle fusion has not been reported.

Table 2. Final (m_{fin}) and critical mass (m_Θ), number of liposomes per unit area ($n_{liposomes}$) and critical surface coverage (Θ) for POPC/POPE SUV with and without QDs deposited on the PEI monolayer.

QD Diameter d	No QD	2.7 nm	3.8 nm	4.9 nm	5.4 nm
m_{fin} (ng cm^{-2})	2995±54	3838±44	2905±19	2101±66	1907±54
m_Θ (ng cm^{-2})	5284±45	4493±160	3594±14	3436±267	3216±19
n_L ($\times10^9$ cm^{-2})	13.90±3.10	6.64±1.94	5.18±1.50	4.78±1.44	4.62±1.34
A ($\times10^3$ nm^2)	7.19±1.61	15.06±4.42	19.32±5.61	20.92±6.31	21.63±6.28
Θ	0.89±0.11	0.63±0.09	0.49±0.07	0.45±0.07	0.44±0.06

AFM imaging was performed to observe the effect of the embedded QDs on the SLB morphology (Figure 5). Compared to the morphology of SLBs without QDs, the embedding of hydrophobic QDs caused the lipid bilayer to appear rougher and patchier, and such structural disruption appeared more pronounced as the QD size increased, with roughness R_a = 0.37, 0.31, 0.39 and 0.72 nm for the bilayer containing QDs of *d* = 2.7, 3.8, 4.9 and 5.4 nm, respectively. This agrees with QCM measurements that the liposomes with larger QDs showed the lowest frequency shift upon vesicle rupture, and the subsequent formation of larger areas of supported lipid bilayer. AFM has been previously used to study interactions between nanoparticles and SLBs.[72] It was shown that NPs could strongly interact with lipid membranes, either by adsorbing onto the membrane surface or penetrating the membrane, depending on the NP physical characteristics and SLB nature.[36,73] However, AFM imaging has not been previously reported for QD-embedded SLBs.

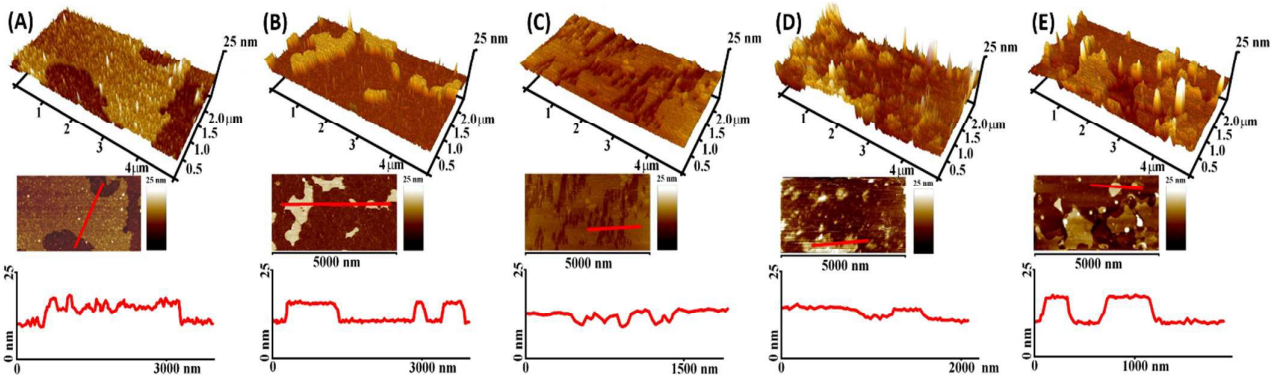

Figure 5. AFM images and line profiles of deposited POPC/POPE SUVs without QDs (A); with 2.7 nm (B); 3.8 nm (C); 4.9 nm (D); 5.4 nm (E) QDs on the top of a PEI monolayer. All the height scale bars in the Figure represent 25 nm.

View Article Online
DOI: 10.1039/C8NR05877F

Nanoscale

ARTICLE

The bilayer thicknesses determined by AFM are listed in **Table 3**, which are slightly thicker than the XRR bilayer thickness (see below). This discrepancy could arise from two sources. First, it is likely that the sharp AFM tip could penetrate through the underlying PEI cushion. In **Table 3**, the total thicknesses including the fitted PEI layer from XRR are also listed, which show a closer agreement with the AFM results. Secondly, the AFM imaging revealed micromorphology (4 µm×2 µm), whereas XRR measurement averages over a much larger footprint
(1 mm×100 µm) and thus is more representative of the average thickness over the whole sample area.[74]

CdS diameter d (nm)	Thickness *t* (nm) (± 0.05 nm)		
	AFM	XRR (bilayer without PEI)	XRR (bilayer plus PEI layer)
No QD	5.54	3.37	4.27
2.7	6.71	4.31	5.24
3.8	5.39	5.17	6.10
4.9	4.25	4.38	5.57
5.4	7.93	4.89	5.85

Table 3. Comparison of AFM and XRR thickness of deposited POPC/POPE SUVs without or with QDs (d = 2.7–5.4 nm) on the top of a PEI monolayer.

XRR measurements revealed the out-of-plane structure of the SLBs. Figure 6 shows XRR curves of POPC/POPE lipid bilayers with and without d = 2.7 nm, 3.8 nm, 4.9 nm and 5.4 nm QDs at 3 h incubation time along with the respective SLD profiles used for fitting the XRR profiles. The Kiessig fringes were most pronounced in the case of the POPC/POPE lipid bilayers. When the QDs were embedded into POPC/POPE lipid bilayers, XRR showed significant changes in both the SLB thickness and SLD values. The XRR profiles for SLBs with 3.8 nm and 4.9 nm CdS QDs exhibited relatively more pronounced fringes compared to those with 2.7 nm and 5.4 nm QDs.

The structural parameters obtained from the analysis of XRR data are included in the SI section SI.5. The thickness of the POPC/POPE bilayers was calculated to be t = 3.4 nm, which indicates a lipid configuration with either tilted or interdigitated hydrophobic chains. In the case of SLB-QDs, the bilayers were thicker, and the surface coverage also increased, due to more densely packed lipid tails. These tendencies clearly indicate the insertion of hydrophobic NPs in the hydrocarbon tail region of the SLBs, and the presence of the hydrophobic QDs also led to denser lipid packing. The highest

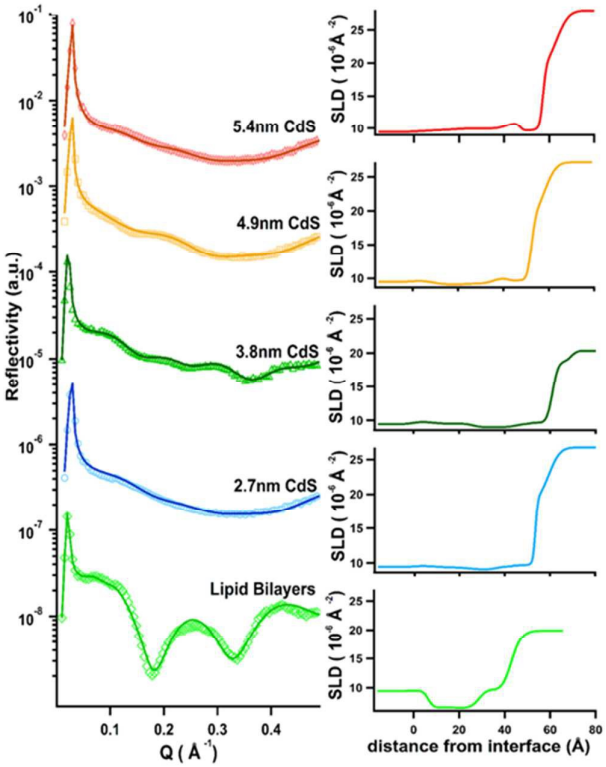

Figure 6. X-ray reflectivity data (left-hand side) and SLD profiles of bilayers without and with QDs. The solid symbols correspond to data and solid lines represent the best fit to the respective data. Reflectivity profiles are shifted vertically for clarity.

value of bilayer thickness (t = 5.17 nm) was observed for 3.8 nm QDs, which can be attributed to the most effective embedding or strong binding of QDs within lipid bilayers. In the case of 2.7 nm, 4.9 nm, and 5.4 nm QDs, the bilayer shows thickness of 4.31 nm, 4.38 nm, and 4.89 nm, respectively.

The interpretation of SLB formation from XRR fitting is consistent from the QCM-D analysis. XRR and QCM-D interrogated and yielded structural information averaged over much larger areas and both point to SLB formation; whereas AFM imaging provided much more localized morphological information. However, it is also possible that liposomes adsorbed atop the bilayer. However, the XRR Kiessig fringes are extremely sensitive to the average surface roughness.[54] Significant liposome presence would result in large surface roughness, which would in turn damp any Kiessig fringes. Therefore, although we cannot rule out liposome adsorption, our XRR data suggests that it would not have been significant.

View Article Online
DOI: 10.1039/C8NR05877F

Conclusions

We have shown that CdS QDs with diameter *d* = 2.7–5.4 nm can be successfully incorporated into alkyl tails region of the POPC/POPE bilayer, as confirmed by cryo-TEM measurements, and that QD fluorescence was retained for both SUVs and SLBs with embedded QDs, evident from their fluorescence emission spectra. The structure of the SLB-QDs was further characterized using synchrotron XRR, providing complementary evidence for QD incorporation into the SLBs. We have found that 3.8 nm and 4.9 nm CdS QDs were optimal to be embedded within membrane bilayers. Furthermore, we have studied the effect of the hydrophobic NPs on the lipid bilayer formation and the final structure of bilayer-QDs hybrids. We have found that the critical surface liposomal coverage (at which fusion occurs) was reached faster for SUV-QDs as compared with liposomes without QDs. Such faster kinetics indicates that QDs promoted fusion, an effect that was more pronounced for larger QDs. AFM imaging revealed that the incorporation of QDs caused disruption of the bilayer structure, again with the bilayers embedded with the larger QDs appearing rougher and patchier with larger surface coverage. Whilst XRR and QCM-D results consistently pointed to the formation of SLBs, complementary AFM imaging revealed patchiness in the SLB micromorphology, suggesting incomplete formation of SLBs. It is also possible that unruptured liposomes adsorbed atop bilayer; however, the observation of the XRR Kiessig fringes indicates that such adsorption would not have been significant.

While SUV-QDs have been widely studied, reports on the characterization of supported bilayers embedded with QDs are limited. Our findings provide useful information on the structure of the fluorescent SLBs incorporating QDs, and also give mechanistic insights into how the QD size could affect the formation kinetics of these SLB-QDs *via* the liposome fusion route. SLB-QDs hybrids represent a promising platform for fluorescence visualization and biosensing in biotechnology.

Conflicts of interest

"There are no conflicts to declare".

Acknowledgements

The work presented was financed by the National Science Centre, Contract No. DEC-2015/19/N/ST4/00917. The European Union Erasmus+ programme (project number: 2016-1-PL01-KA103-023786) is acknowledged for providing scholarship (financial support) for the research/mobility/traineeship. W.H.B. would like to acknowledge funding from the EPSRC (EP/H034862/1, EP/G036780/1, EP/L016648/1, EP/K502996/1, EP/J500379/1) and Marie Curie Initial Training Network (MCITN) on "Soft, Small, and Smart: Design, Assembly, and Dynamics of Novel Nanoparticles for Novel Industrial Applications" (NanoS3; Grant No. 290251). S.K. acknowledges GAČR grant 18-25144Y. L.I. is funded by the Consejo Nacional de Ciencia y Tecnologia (CONACyT) Postdoctoral Fellowship 291231. XMaS is a mid-range facility supported by EPSRC (UK). We are grateful to all the beam line team staff for their support.

References

1 M. Hofmann-Amtenbrink, D. W. Grainger and H. Hofmann, *Nanomedicine Nanotechnology, Biol. Med.*, 2015, **11**, 1689-1694.
2 J. M. Bulpett, A. M. Collins, N. H. M. Kaus, P. T. Cresswell, O. Bikondoa, D. Walsh, S. Mann, S. a. Davis and W. H. Briscoe, *J. Mater. Chem.*, 2012, **22**, 15635-15643.
3 A. Pajor-Swierzy, M. Kolasinska-Sojka and P. Warszynski, *Colloid Polym. Sci.*, 2014, **292**, 455-465.
4 Y. Chen, A. Bose and G. D. Bothun, *ACS Nano*, 2010, **4**, 3215-3221.
5 N. V. Beloglazova, P. S. Shmelin, E. S. Speranskaya, B. Lucas, C. Helmbrecht, D. Knopp, R. Niessner, S. De Saeger and I. Y. Goryacheva, *Anal. Chem.*, 2013, **85**, 7197-7204.
6 V. De Leo, L. Catucci, A. Falqui, R. Marotta, M. Striccoli, A. Agostiano, R. Comparelli and F. Milano, *Langmuir*, 2014, **30**, 1599-1608.
7 M. kyung So, H. Yao and J. Rao, *Biochem. Biophys. Res. Commun.*, 2008, **374**, 419-423.
8 X. Gao, Y. Cui, R. M. Levenson, L. W. K. Chung and S. Nie, *Nat. Biotechnol.*, 2004, **22**, 969-976.
9 P. Zrazhevskiy, M. Sena and X. Gao, *Chem. Soc. Rev.*, 2010, **39**, 4326-4354.
10 J. K. Jaiswal, E. R. Goldman, H. Mattoussi and S. M. Simon, *Nat. Methods*, 2004, **1**, 73-78.
11 I. L. Medintz, H. T. Uyeda, E. R. Goldman and H. Mattoussi, *Nat. Mater.*, 2005, **4**, 435-446.
12 E. Lewis, S. Haigh and P. O'Brien, *J. Mater. Chem. A*, 2014, **2**, 570-580.
13 A. Valizadeh, H. Mikaeili, M. Samiei, S. M. Farkhani, N. Zarghami, M. Kouhi, A. Akbarzadeh and S. Davaran, *Nanoscale Res. Lett.*, 2012, **7**, 480.
14 N. Chen, Y. He, Y. Su, X. Li, Q. Huang, H. Wang, X. Zhang, R. Tai and C. Fan, *Biomaterials*, 2012, **33**, 1238-1244.
15 M. Walling, J. Novak and J. R. E. Shepard, *Int. J. Mol. Sci.*, 2009, **10**, 441-91.
16 K. Tahara, S. Fujimoto, F. Fujii, Y. Tozuka, T. Jin and H. Takeuchi, *J. Pharm.*, 2013, **2013**, 1-6.
17 J. Y. Wang, J. F. Zhao, P. N. Wang, W. L. Yang and J. Y. Chen, *J. Fluoresc.*, 2011, **21**, 1635-1642.
18 M. R. Rasch, E. Rossinyol, J. L. Hueso, B. W. Goodfellow, J. Arbiol and B. A. Korgel, *Nano Lett.*, 2010, **10**, 3733-3739.
19 H. S. Wi, K. Lee and H. K. Pak, *J. Phys. Condens. Matter*, 2008, **20**, 494211.
20 V. V. Ginzburg and S. Balijepalli, *Nano Lett.*, 2007, **7**, 3716-3722.
21 L. Feng, X. Kong, K. Chao, Y. Sun, Q. Zeng and Y. Zhang, *Mater. Chem. Phys.*, 2005, **93**, 310-313.
22 J. Batalla, H. Cabrera, E. San Martín-Martínez, D. Korte, A. Calderón and E. Marín, *Biomed. Opt. Express*, 2015, **6**, 3898-906.
23 G. D. Bothun, A. E. Rabideau and M. A. Stoner, *J. Phys. Chem. B*, 2009, **113**, 7725-7728.
24 R. B. Lira, M. A. B. L. Seabra, A. L. L. Matos, J. V. Vasconcelos, D. P. Bezerra, E. de Paula, B. S. Santos and A. Fontes, *J. Mater. Chem. B*, 2013, **1**, 4297-4305.
25 J. H. Liu, L. Cao, G. E. LeCroy, P. Wang, M. J. Meziani, Y. Dong, Y. Liu, P. G. Luo and Y. P. Sun, *ACS Appl. Mater. Interfaces*, 2015, **7**, 19439-19445.
26 X. Zhang and S. Yang, *Langmuir*, 2011, **27**, 2528-2535.
27 V. K. Komarala, Y. P. Rakovich, A. L. Bradley, S. J. Byrne, S. A. Corr and Y. K. Gun'Ko, *Nanotechnology*, 2006, **17**, 4117-4122.
28 I. Bruzas, S. Unser, S. Yazdi, E. Ringe and L. Sagle, *Anal. Chem.*,

View Article Online
DOI: 10.1039/C8NR05877F

2016, **88**, 7968-7974.
29 A. R. Ferhan, G. J. Ma, J. A. Jackman, T. N. Sut, J. H. Park and N. J. Cho, *Sensors*, 2017, **17**, 1-18.
30 M. J. Murcia, D. E. Minner, G. M. Mustata, K. Ritchie and C. A. Naumann, *J. Am. Chem. Soc.*, 2008, **130**, 15054-15062.
31 C. M. Beddoes, C. P. Case and W. H. Briscoe, *Adv. Colloid Interface Sci.*, 2015, **218**, 48-68.
32 E. Rascol, J.-M. Devoisselle and J. Chopineau, *Nanoscale*, 2016, **8**, 4780–4798.
33 A. Luchini, Y. Gerelli, G. Fragneto, T. Nylander, G. K. Pálsson, M. S. Appavou and L. Paduano, *Colloids Surfaces B Biointerfaces*, 2017, **151**, 76-87.
34 B. Jing and Y. Zhu, *J. Am. Chem. Soc.*, 2011, **133**, 10983-10989.
35 Y. Li, X. Chen and N. Gu, *J. Phys. Chem. B*, 2008, **112**, 16647-16653.
36 P. R. Leroueil, S. A. Berry, K. Duthie, G. Han, V. M. Rotello, D. Q. McNerny, J. R. Baker, B. G. Orr and M. M. B. Holl, *Nano Lett.*, 2008, **8**, 420-424.
37 J. Q. Lin, H. W. Zhang, Z. Chen, Y. G. Zheng, Z. Q. Zhang and H. F. Ye, *J. Phys. Chem. C*, 2011, **115**, 18991-18998.
38 G. D. Bothun, *J. Nanobiotechnology*, 2008, **6**, 13.
39 S. H. Park, S. G. Oh, J. Y. Mun and S. S. Han, *Colloids Surfaces B Biointerfaces*, 2005, **44**, 117-122.
40 S. H. Park, S. G. Oh, J. Y. Mun and S. S. Han, *Colloids Surfaces B Biointerfaces*, 2006, **48**, 112-118.
41 J. M. Bulpett, T. Snow, B. Quignon, C. M. Beddoes, T.-Y. D. Tang, S. Mann, O. Shebanova, C. L. Pizzey, N. J. Terrill, S. A. Davis and W. H. Briscoe, *Soft Matter*, 2015, **11**, 8789-8800.
42 C. M. Beddoes, J. Berge, J. E. Bartenstein, K. Lange, A. J. Smith, R. K. Heenan and W. H. Briscoe, *Soft Matter*, 2016, **12**, 6049-6057.
43 K. Murzyn, T. Róg and M. Pasenkiewicz-Gierula, *Biophys. J.*, 2005, **88**, 1091-1103.
44 N. Kučerka, N. Kučerka, F. A. Heberle, J. Pan and J. Katsaras, *Membranes*, 2015, **5**, 454-472.
45 D. A. Pink, S. McNeil, B. Quinn and M. J. Zuckermann, *Biochim. Biophys. Acta*, 1998, **1368**, 289-305.
46 M. Wlodek, M. Szuwarzynski and M. Kolasinska-Sojka, *Langmuir*, 2015, **31**, 10484-10492.
47 M. Kolasinska, R. Krastev and P. Warszynski, *J. Colloid Interface Sci.*, 2007, **305**, 46-56.
48 M. Kolasinska, R. Krastev, T. Gutberlet and P. Warszynski, *Progress in Colloid and Polymer Science*, 2007, **134**, 30-38.
49 M. Wlodek, M. Kolasinska-Sojka, M. Wasilewska, O. Bikondoa, W. H. Briscoe and P. Warszynski, *Soft Matter*, 2017, **13**, 7848-7855.
50 M. Wlodek, M. Kolasinska-Sojka, M. Szuwarzynski, S. Zapotoczny and P. Warszynski, *Thin Solid Films*, 2015, **592**, 1-7.
51 Z. Adamczyk, A. Michna, M. Szaraniec, A. Bratek and J. Barbasz, *J. Colloid Interface Sci.*, 2007, **313,** 86-96.
52 https://www.biolinscientific.com/qsense,
53 W. H. Briscoe, M. Chen, I. E. Dunlop, J. Klein, J. Penfold and R. M. J. Jacobs, *J. Colloid Interface Sci.*, 2007, **306**, 459-463.
54 F. Speranza, G. A. Pilkington, T. G. Dane, P. T. Cresswell, P. Li, R. M. J. Jacobs, T. Arnold, L. Bouchenoire, R. K. Thomas and W. H. Briscoe, *Soft Matter*, 2013, **9**, 7028-7041.
55 W. H. Briscoe, F. Speranza, P. Li, O. Konovalov, L. Bouchenoire, J. van Stam, J. Klein, R. M. J. Jacobs and R. K. Thomas, *Soft Matter*, 2012, **8**, 5055-5068.
56 B. Sironi, T. Snow, C. Redeker, A. Slastanova, O. Bikondoa, T. Arnold, J. Klein and W. H. Briscoe, *Soft Matter*, 2016, **12**, 3877-3887.
57 A. Nelson, *J. Appl. Crystallogr.*, 2006, **39**, 273-276.
58 W. T. Al-Jamal, K. T. Al-Jamal, B. Tian, L. Lacerda, P. H. Bornans, P. M. Frederik and K. Kostarelos, *ACS Nano*, 2008, **2**, 408-418.
59 V. R. Kethineedi, G. Crivat, M. A. Tarr and Z. Rosenzweig, *Anal. Bioanal. Chem.*, 2013, **405**, 9729-9737.
60 https://www.sigmaaldrich.com/catalog/product/aldrich/662593?lang=pl&region=PL&cm_sp=Insite-_-prodRecCold_xviews-_-prodRecCold10-7
61 R. Kumar, A. Kulkarni, D. K. Nagesha and S. Sridhar, *Theranostics*, 2012, **2**, 714-722.
62 M. Noh, T. Kim, H. Lee, C. K. Kim, S. W. Joo and K. Lee, *Colloids Surfaces A Physicochem. Eng. Asp.*, 2010, **359**, 39-44.
63 C. R. González Vargas, J. Douda, A. A. Vallejo Cardona and J. L. Casas Espinola, *Front. Sensors*, 2016, **4**, 27-32.
64 C. Ye, Y. Wang, C. Li, J. Yu and Y. Hu, *Microchim. Acta*, 2013, **180**, 117-125.
65 S. Kumar, M. Gradzielski and S. K. Mehta, *RSC Adv.*, 2013, **3**, 2662-2676.
66 R. Michel and M. Gradzielski, *Int. J. Mol. Sci.*, 2012, **13**, 11610-11642.
67 C. Montis, V. Generini, G. Boccalini, P. Bergese, D. Bani and D. Berti, *J. Colloid Interface Sci.*, 2018, **516**, 284-294.
68 R. P. Richter, R. Bérat and A. R. Brisson, *Langmuir*, 2006, **22**, 3497-3505.
69 R. P. Richter and A. R. Brisson, *Biophys. J.*, 2005, **88**, 3422-3433.
70 T. K. Lind and M. Cárdenas, *Biointerphases*, 2016, **11**, 020801.
71 N. Yousefi and N. Tufenkji, *Front. Chem.*, 2016, **4**, 46.
72 Y. Roiter, M. Ornatska, A. R. Rammohan, J. Balakrishnan, D. R. Heine and S. Minko, *Nano Lett.*, 2008, **8**, 941-944.
73 N. Biswas, R. Bhattacharya, A. Saha, N. R. Jana and J. K. Basu, *Phys. Chem. Chem. Phys.*, 2015, **17**, 24238-24247.
74 L. Zhou, L. Fox, W. Magdalena, L. Islas, A. Slastanova, E. Robles, O. Bikondoa, R. Harniman, N. Fox, M. Cattelan and W. H. Briscoe, *Carbon*, 2018, **136**, 255-261.

View Article Online
DOI: 10.1039/C8NR05877F